Advances in Engineering Software 101 (2016) 98–105

Contents lists available at ScienceDirect

Advances in Engineering Software

journal homepage: www.elsevier.com/locate/advengsoft

The Mach stem phenomenon for shaped obstacles buried in soil

Y.S. Karinski, V.R. Feldgun, E. Racah, D.Z. Yankelevsky*

National Building Research Institute, Technion-Israel Institute of Technology, Haifa 32000, Israel

ARTICLE INFO

Article history:
Available online 9 February 2016

Keywords:
Soil–structure interaction
Shock wave
Mach stem
Nearby explosion
Shaped obstacle

ABSTRACT

The paper investigates the explosion characteristics of a below ground event of an explosive charge in proximity to a rigid cylindrical obstacle. The two-dimensional study simulates a line explosive and a parallel long cylindrical structure. The investigation shows that the unloading branch has a negligible effect on the peak pressure envelope whereas shear behavior and explosives burning have a considerable effect and should not be disregarded. The effect of the soil's equation of state and especially the full locking parameter on the pressure distribution on an obstacle has been studied. At a short standoff distance where a steep pressure growth beyond the full compaction point is developed, the pressure distributions envelope shows three maxima values that are located at some distance away from the axis of symmetry. It is different than the common single peak along the axis, in the case of a distant explosion. This effect is more pronounced for a medium having sharper pressure growth in the EOS beyond the full compaction point and for smaller charge standoff distances. The pressure distributions analysis indicates that the appearance of second (absolute-primary) and third (secondary) peaks are caused by the Mach stem effect appearing in a soil medium with full locking. The secondary peak pressure envelope maximum corresponds to the secondary Mach stem phenomenon that does not appear in the case of a planar wall, where the incident angle depends on the wave front curvature only.

1. Introduction

The problem of an underground explosion near a buried structure is of much interest and of great complexity [1–3]. It combines the shock wave propagation and its interaction with a buried structure, as well as the accompanied rather large soil deformations and the formation of an explosive cavity in soil [4,5] and the structures dynamic response. The shock wave propagation in soil is rather complex, and should follow on a highly nonlinear constitutive model [4,6,7]. Commonly rather simple models are used to represent the soil medium behavior, such as elastic [8,9] or elastic plastic with elastic volumetric deformation [10–12]. However, proper representation of the soil behavior should account for the bulk irreversible compaction [6,13]. When the explosive source is placed at a large distance from the buried structure, the incident shock wave action on the structure may be approximated by a plane wave [14]. For this simple case an analytical solution may be provided [1,5]. When the explosive is placed closer to the structure, the incident wave front must be considered as a spherical or a cylindrical wave, depending on the explosive's and the problem's geometry [15,16] and when the explosive is placed very close to the structure the interaction of the explosive cavity with the obstacle (i.e. the shock wave front distortion) must be taken into account [17,18]. The interaction problems of soils and structures are commonly solved by utilizing numerical methods such as finite element [9–11], finite difference [19], finite volumes [20], variational difference [21] and various coupled methods [12–22,23].

In earlier studies [17,18] the authors presented the variational difference method and its application to the analysis of an explosion in an infinite medium [18] and inside a buried lined cavity [17]. In recent works [24,25] this approach was implemented to analyze a deeply buried explosion of cylindrical charges in a compressible elastic plastic soil that occurs in proximity to a vertical rigid wall and found that when the explosion is relatively close to the wall, the envelope of the pressure distributions (connecting the maximum stress values of the pressure distributions at all times) shows a maximum value that is located at some distance away from the plane of symmetry and not along the plane of symmetry as is commonly the case in a distant explosion. It has been sown that this phenomenon is caused by the Mach stem effect appearing in a soil medium with significant hardening. The present paper considerably extends the investigation of [24,25] to shaped obstacles and is based on the original conference paper [26].

* Corresponding author. Tel.: +972 48293187; fax: +972 8324535.
E-mail address: karinski@tx.technion.ac.il (D.Z. Yankelevsky).

http://dx.doi.org/10.1016/j.advengsoft.2016.01.011
0965-9978/

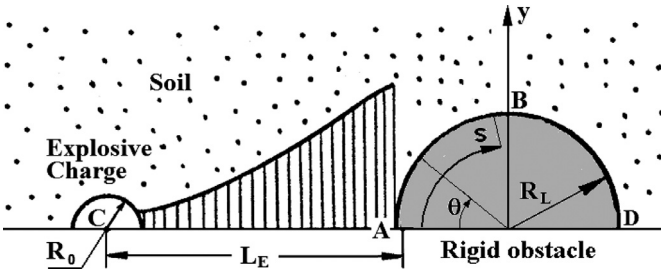

Fig. 1. The problem.

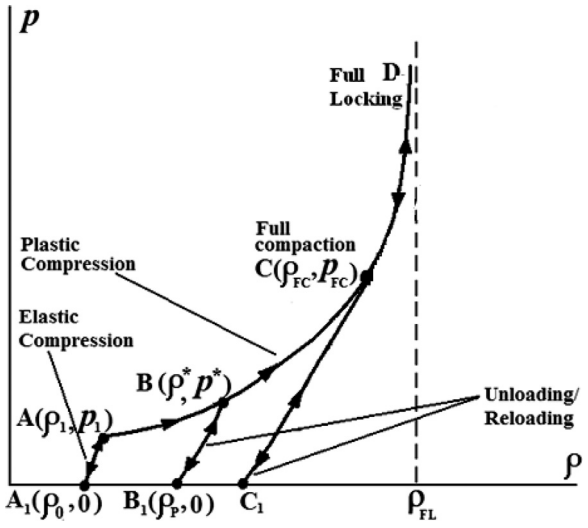

Fig. 2. Pressure–density relationship.

2. The model

Consider a line-charge explosion near a shaped (circular cross section) rigid obstacle (Fig. 1) that is buried in a homogeneous isotropic irreversibly compressible soil medium.

The pressure–density relationship is schematically shown in Fig. 2. The bulk behavior of this material starts with a linear elastic segment (A_1A) that is small and generally can be disregarded, especially when high pressures are considered. This elastic segment is followed by a zone of elastic plastic bulk compaction (segment ABC) with stiffening caused by the closure of the internal pores. A linear or non-linear elastic model (segments B_1B, C_1C) ABC represents unloading and reloading at this stage. The unloading line is uniquely determined by the maximum soil density ρ^* that is attained in the process of active loading. This irreversible process occurs as long as the density is smaller than the full compaction value ρ_{FC} (point C) corresponding to the full closure of the internal pores. Thereafter the pressure varies with the density according to a non-linear elastic behavior (segment CD). This zone corresponds to a constant ρ^* equal to a full compaction density and therefore during the entire process $\rho_1 \le \rho^* \le \rho_{FC}$. The model allows describing the range of pressure values from low pressures (for the case of a far explosion) to very high pressures (for the case of a nearby explosion).

The soil pressure–density relationship takes the form (see Fig. 2):

$$p = f(\rho,\ \rho^*) = \begin{cases} f_L(\rho) & \text{for the active loading} \quad (A_1ABCD) \\ f_U(\rho,\ \rho^*) & \text{for unloading and reloading } (B_1B,\ C_1C) \end{cases} \tag{1}$$

where ρ is the soil current density.

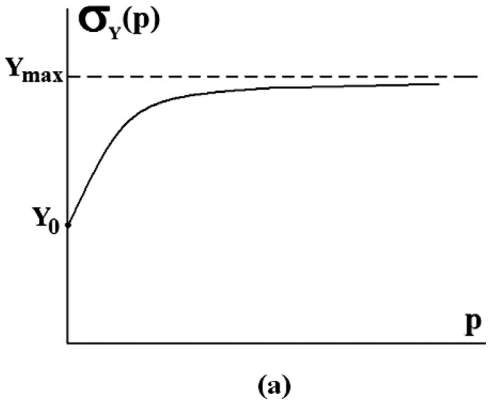

Fig. 3. Yield stress–pressure relationship.

The functions f_L and f_U of Eq. (1) depend on the type of the soil and may be obtained from dynamic compression tests.

The paper examines the medium having a full locking branch (C-D) with the following functions of equation of state [24]:

$$f_L(\rho) = \rho_0 c_0^2 \frac{\varepsilon_V}{(1-\beta\varepsilon_V)^2};$$
$$f_U(\rho,\ \rho^*) = f_L(\rho^*) + c_U^2(\rho^*)(\rho - \rho^*);$$
$$c_U(\rho^*) = c_{FC} + \frac{\rho_{FC} - \rho^*}{\rho_{FC} - \rho_0}(c_0 - c_{FC}) \tag{2}$$

Here ρ_0 and c_0 are the initial density and sound velocity, $\varepsilon_V = 1 - \rho_0/\rho$ is the bulk strain ($0 \le \varepsilon_V < 1/\beta$), c_0 is an initial sound velocity, $1/\beta$ is a full locking bulk strain (Fig. 2), $c_U(\rho^*)$ is the current sound velocity and $c_{FC} = \sqrt{df_L(\rho)/d\rho|_{\rho=\rho_{FC}}}$ is the sound velocity at the state of full compaction. The model assumes that the soil has no tensile resistance. Therefore, if during unloading from a compression state of stress the soil density reaches a permanent density ρ_p (Fig. 2), that corresponds to a zero hydrostatic stress, a discontinuity in the soil occurs and all the stresses (both spherical and deviatoric components) drop to zero. This type of equation of state is typical for soils with high level of bulk hardening at for high pressures (such as clay or clay loam) [4,16,18,23,24].

The Lundborg model [18] is used to describe the yield condition (see Fig. 3):

$$S_{ij}S_{ij} = \frac{2}{3}\sigma_Y^2(p);\ \sigma_Y(p) = Y_0 + \mu_Y p/(1 + \mu_Y p/(Y_{\max} - Y_0)) \tag{3}$$

where Y_0 is the shear cohesion, μ_Y is an internal friction coefficient and $Y_{\max}$ is the shear strength.

The calculations have been performed using either a home-made program that is described in detail in [18,24] and the commercial software AUTODYN-13. Both programs show similar results.

3. The charge explosion in proximity to cylindrical obstacle

Consider the response of a rigid cylindrical obstacle of radius $R_L = 0.5$ m (Fig. 1). The obstacle is buried in soil and subjected to an external explosion of a line TNT charge of radius $R_0 = 10$ cm that is placed at a depth of $H = 3.6$ m below the soil top surface, and at a distance L_E from the lining front (point A, Fig. 1). Note, that both the obstacle and the charge are buried deep enough in the soil to avoid any free surface effects including the free surface cratering.

A recent study [25] examined the peak pressure distribution for both planar and cylindrical obstacles (peak pressure envelop). It shows that for a nearby explosion the maximum value of the peak pressure envelope is developed somewhat away from the plane of

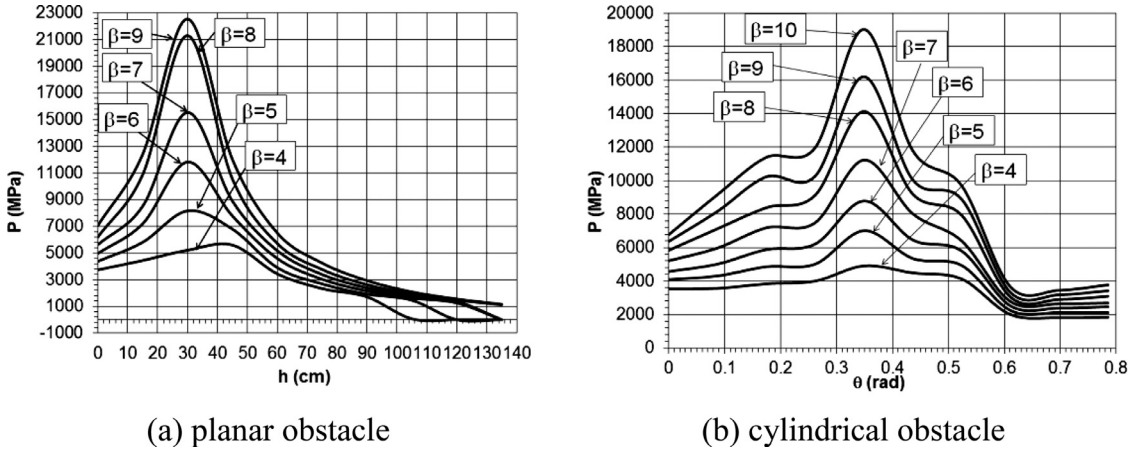

Fig. 4. Peak pressure envelope for a nearby explosion ($L_E = 5R_0$) (a) planar obstacle (b) cylindrical obstacle.

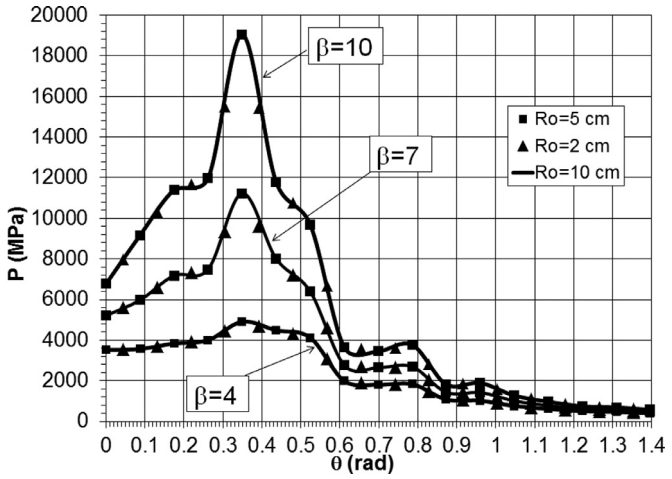

Fig. 5. Scaling.

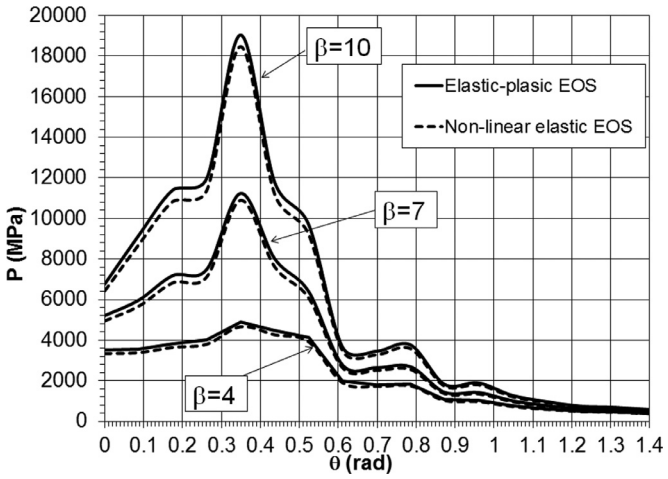

Fig. 6. Effect of unloading.

symmetry for both planar and cylindrical obstacles (Fig. 4). This phenomenon is more pronounced for larger values of the full locking parameter β (see Eq. (2)).

However the shapes of the peak pressure envelopes of the two obstacles are qualitativly different: the planar obstacle envelope has one peak only (Fig. 4a), whereas the shaped obstacle envelope has three peaks (Fig. 4b): the primary peak is developed at about 0.25 rad and 2 secondary peaks are developed at about 0.2 and 0.5 rad. The present paper aims at analyzing and explaining that 3-peak observation.

A comprehensive account of Mach reflection over a 2D cylindrical convex surface is given in Ref. [27]. This account is limited to Mach reflections in gases and doesn't deal with soils or any other solid. It is shown that a shock reflection over a cylindrical surface undergoes consecutively the following regimes: regular reflection (RR), double Mach (DMR), transitional Mach (TMR) and single Mach (SMR).

It is very tempting to identify the three peaks of Figs. 4b and 5 with the three different Mach reflections DMR, TMR and SMR. One should be careful, however, because in order to get a positive identification with these definitions in soils, much more refined numerical simulations are needed. Such refined simulations should be able to distinguish the different branches of DMR and TMR and are beyond the scope of this paper.

4. Parametric study

4.1. Geometric scaling

To validate the geometric scaling, the analysis has been carried out for different values of the full locking parameter ($\beta = 4$, 7 and 10 that represent minimum, average and maximum values of the investigated problem – Fig. 4a) and for the following charge and obstacle radii : $R_0 = 10$ cm, $R_L = 50$ cm (reference case), $R_0 = 5$ cm, $R_L = 25$ cm (geometric scaling factor is 0.5) and $R_0 = 2$ cm, $R_L = 10$ cm (geometric scaling factor is 0.2). The mesh size for the numerical analysis was reduced proportionally to the geometric scaling factor. Fig. 5 shows the computed results for the three scales and very good correspondence is observed (the maximum difference is less than 1%).

4.2. Unloading branch

Unloading/reloading strongly affects the behavior much after the shock wave front meets the obstacle. However, the peak pressure envelope is formed by interaction of the wave shock front with the obstacle and therefore is not likely to be affected by the shape of the unloading curve. To examine this aspect, a comparison is carried out between two equations of state: an elastic–plastic relationship, with unloading/reloading that is different from the active loading line (as is fully described by Eqs. 2) and a non-linear

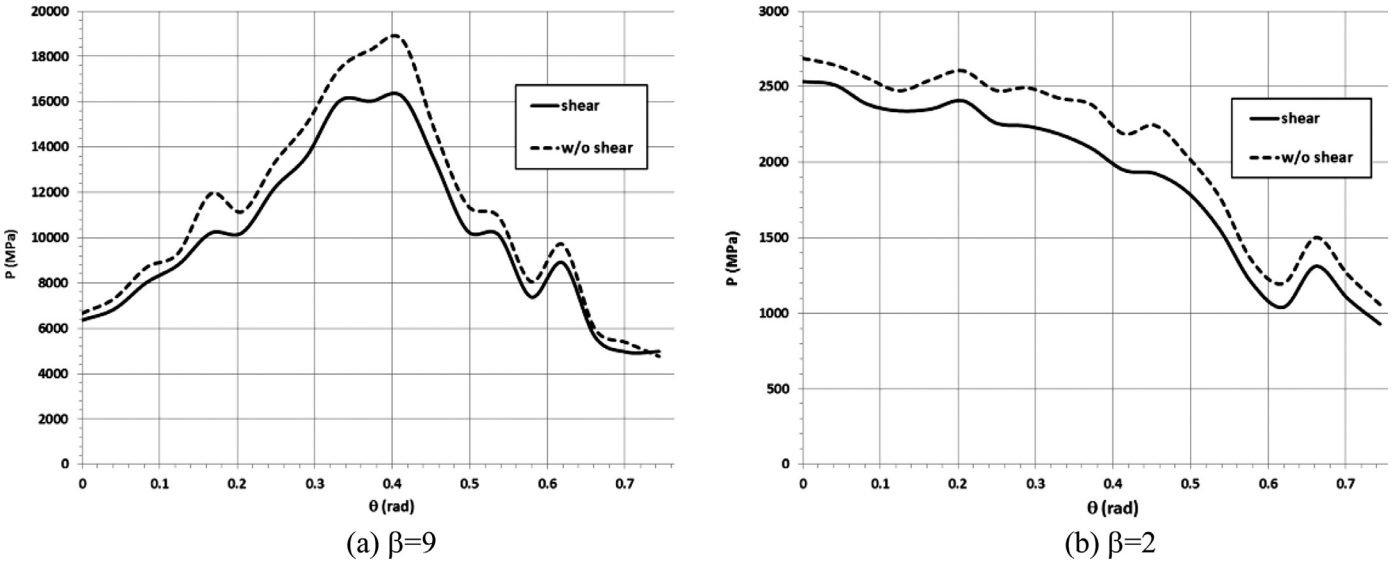

Fig. 7. Effect of shear behavior ($L_E = 5R_0$) (a) $\beta = 9$ (b) $\beta = 2$.

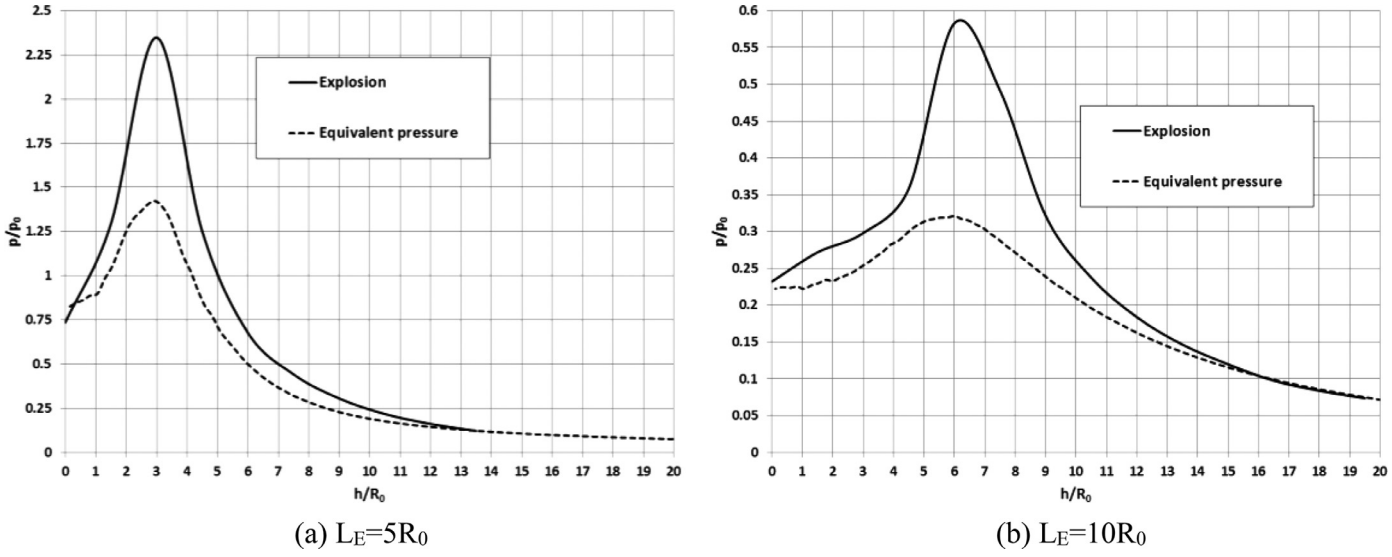

Fig. 8. Effect of explosion imitation – vertical wall (a) $L_E = 5R_0$ (b) $L_E = 10R_0$.

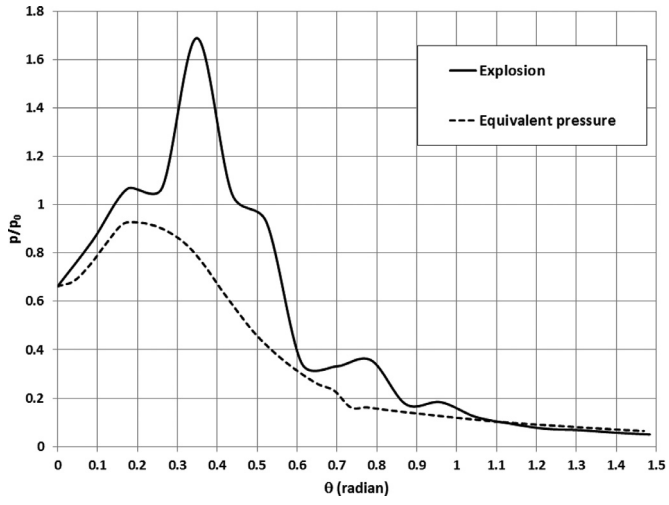

Fig. 9. Effect of explosion initiation – cylindrical obstacle.

elastic relationship, for which the unloading/reloading curve coincides with the active loading (according to the first of Eq. (2)). The comparisons were perfomed for the same three values of full locing parameters: $\beta = 4, 7, 10$. Fig. 6 shows the results of the analysis and the negligible efffect of the unloading branch on the evaluation of the peak pressure envelope is clearly shown (the maximum error does not exeed 5%).

4.3. Deviatoric behavior

In contrary to a gas dynamics where the Mach stem effect is well known, the soil medium response is characterized not only by the equation of state but also by the medium shear behavior. To examine the effect of the shear (deviatoric) behavior on the peak pressure envelope two models are examined in the following: a complete model that is described above (Eqs. (2) and (3)) and a "plastic gas" model which takes into consideration only the equation of state (Eq. (2)). Fig. 7 shows comparisons for two values of the full locking parameter: a large value ($\beta = 9$), corresponding to 3-peak type envelope, and a small value ($\beta = 2$), for which a single peak value is obtained at the axis of symmetry. A

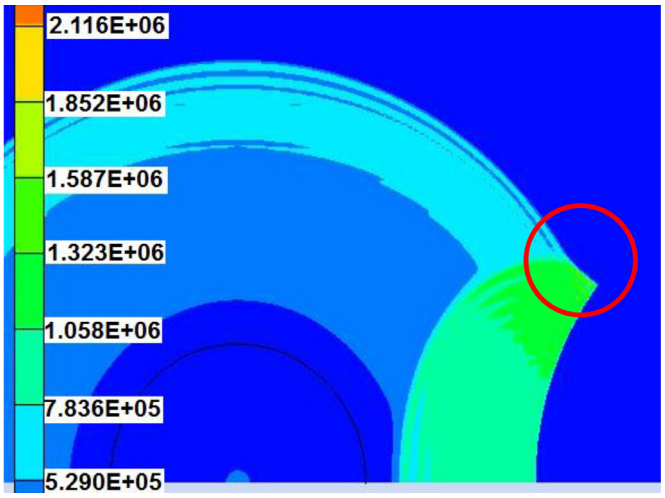

Fig. 10. Contact pressure field, $\beta = 4$ – Triple point.

significant quantitative difference between the results is observed, although there exists a qualitative similarity. The relative difference of the peak pressure magnitude varied from 6% for $\beta = 2$ to 15% for $\beta = 9$. Similar results were obtained for other values of the full locking parameter and of the charge-obstacle standoff distance.

4.4. Modeling of the explosion

Distant explosions are often simulated by an initial internal pressure in a representative explosive's cavity [28]. In this case the initial fields of the gas dynamics parameters (density ρ_H, pressure p_H and velocities u_H) are obtained by solving the detonation problem described by the Chapman–Jouget model [29]. The following pressure $p_D(t)$ is calculated as:

$$p_D = p_H \left(\frac{\rho_D}{\rho_H} \right)^3 \tag{4}$$

where ρ_D is the current density of the explosive products obtained by using the charge mass conservation law:

$$A_D(t)\rho_D(t) = \pi R_E^2 \rho_H, \tag{5}$$

A_D is the current charge cross section area.

This is an oversimplified approach to describe a nearby explosion and the JWL equations of state of the explosive should be used instead including consideration of the explosives burning [30]. A study of these two alternative representations of similar problems has been carried out for several different scaled distances (that measure that distance between the explosive and the obstacle by explosive's radii). It was found that for a relatively distant charge ($L_E > 30R_0$) the results are identical. However for a nearby explosion the results are considerably different from each other as sown in Figs. 8 and 9. The simplified approach predicts well the contact pressure at the frontal point (located at the axis of symmetry) as well as along the distant parts of the obstacles ($h/R_0 > 12$ for the rigid wall and $\theta > 60°$ for the rigid cylinder). For a

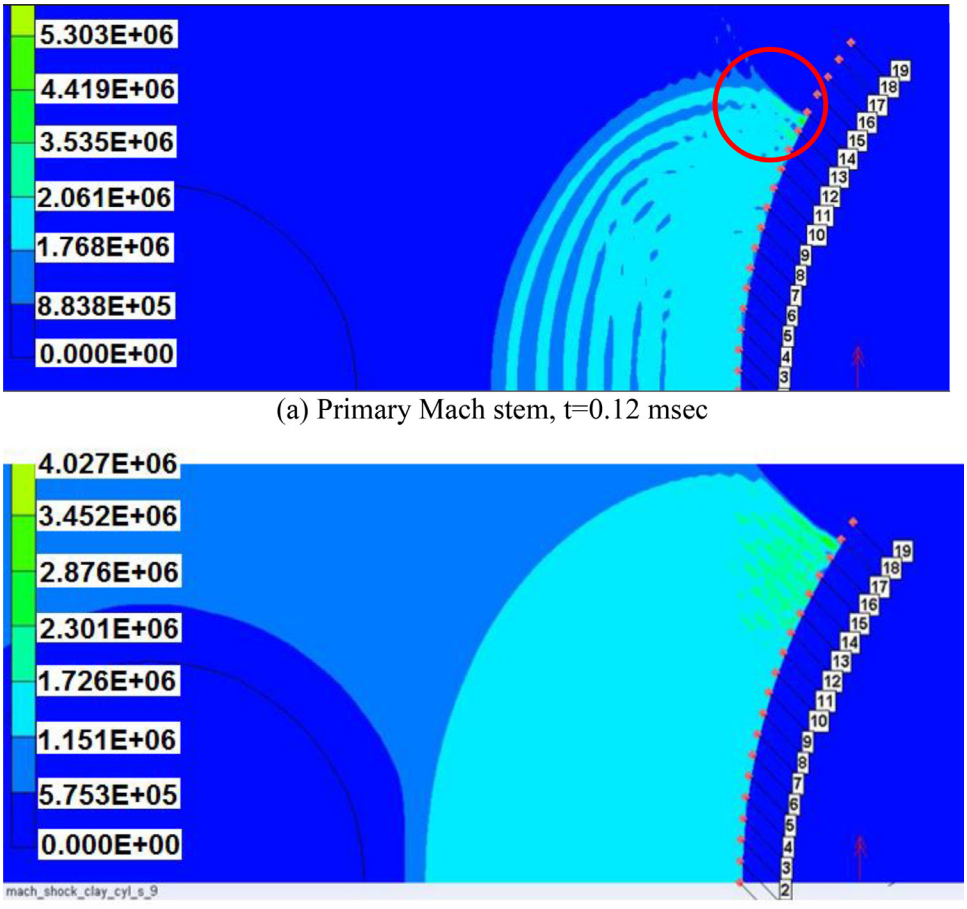

(a) Primary Mach stem, t=0.12 msec

(b) Secondary Mach stem, t=0.13 msec

Fig. 11. Contact pressure field $\beta = 9$. (a) Primary Mach stem, $t = 0.12$ ms. (b) Secondary Mach stem, $t = 0.13$ ms.

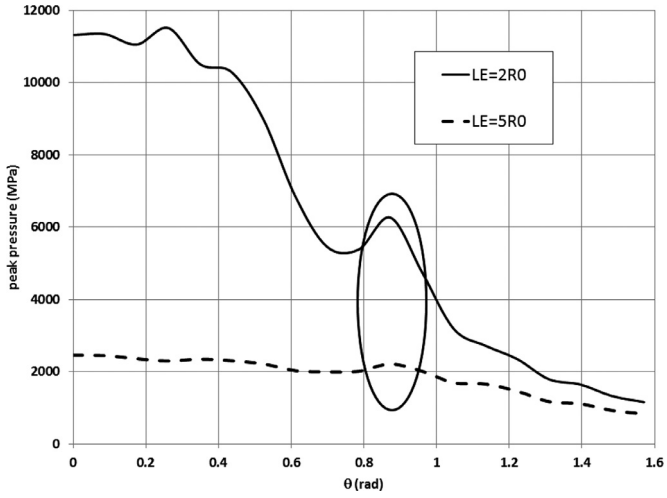

Fig. 12. Peak pressure distribution for various distances; $\beta = 2$.

planar obstacle (Fig. 8) the peak pressure predicted using a simplified approach is smaller by ~40% from the peak pressure obtained by exact burning simulation, although both envelopes are qualitatively similar.

In the case of a shaped obstacle the simplified approach predicts the first pressure peak only (the predicted pressure is ~35% smaller than the pressure prediction using the JWL equation of state). The second (absolute) and third maxima are not predicted by the simplified approach (Fig. 9). Therefore for the pressure envelope prediction along a shaped obstacle due to a nearby explosion only the exact model of explosive burning should be used.

5. Examination of the primary and secondary Mach stems

The following will investigate whether the Mach stem produces these maxima values. Calculations of the contact pressure fields at various time instants were performed using AUTODYN Euler solver with JWL EOS for the TNT domain, "Shock" type of EOS and Drucker–Prager model for shear (strength) simulation.

As stated in Ch. 3, also in AUTODYN, the limited numerical resolution does not allow us to identify the triple points shown in Figs. 10,11,13, and 14 with the specific kind of Mach reflection specified in Ref. [27].

Fig. 10 shows the typical for Mach stem triple point in the pressure fields when the parameters of the equation of state produce the three-peak envelope shape. This Mach stem is developed at the point corresponding to a second (primary) peak of the pressure envelope (see Fig. 4b).

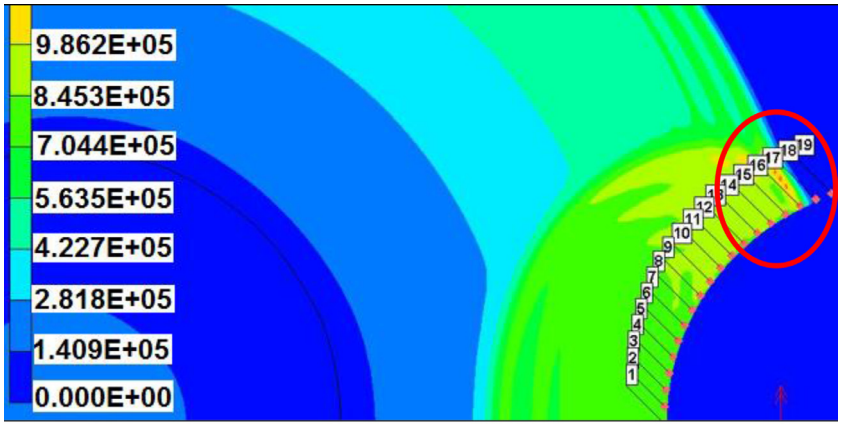

(a) L_E=5R_0, t=0.24 msec

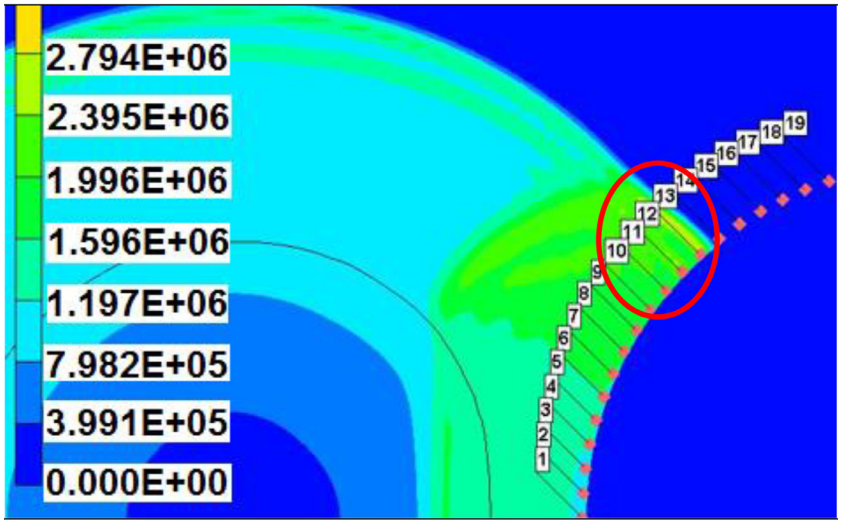

(b) L_E=2R_0, t=0.08 msec

Fig. 13. Secondary Mach stem for $\beta = 2$ (a) $L_E = 5R_0$, $t = 0.24$ ms (b) $L_E = 2R_0$, $t = 0.08$ ms.

Fig. 14. Stress concentration at the point of first peak.

To study the phenomenon of secondary peaks, an analysis of the pressure fields at larger time was carried out. Fig. 11 shows that the Mach stem is first developed at the point, that corresponds to the primary maximum (Fig. 11a) and later it is developed at the point, corresponding to the second secondary maximum (Fig. 11b). Therefore, it may be concluded that this secondary maximum of the peak pressure envelope corresponds to the secondary Mach stem phenomenon that does not appear in the case of a planar wall, where the incident angle depends on the wave front curvature only.

The gauge points (1–19) in Figs. 11,13,14 were used to find the pressure peaks as in Fig. 12.

Decrease of the charge-obstacle distance leads to increase of both the primary and secondary maxima even for relatively small β as may be observed in Fig. 12. The corresponding contact pressure fields are shown in Fig. 13.

The first secondary peak is not accompanied with the Mach stem. At early time some pressure concentration develops at this point (Fig. 14) and disappears at later times. The fact, that the point at which this first maximum is developed is the only point that is predicted by the simplified model (Fig. 9) and that it is not developed for relatively small values of β (Fig. 12), leads to an assumption that this peak is caused by the detailed explosion processes occurring within the explosive cavity. However this phenomenon requires further studies that is beyond the scope of this paper.

6. Conclusions

An investigation of the explosion characteristics of a charge-line explosive in soil in proximity to a rigid cylindrical obstacleburied in soil has been carried out. The soil is modeled as an irreversible compressible medium with full bulk locking and dependence of the current deviatoric yield stress on the pressure.

The parameters study for a nearby explosion shows that the loading branch of the equation of state has a dominant effect on the evaluation of the peak pressure envelope. Consideration of the soil shear behavior and explosives equation of state including the burning pocess have a major effect and should be taken into consideration to obtain a reliable quantitative prediction of the envelope shape.

The pressure distribution along an obstacle has been studied for various values of the medium's full locking parameter. For a short standoff distance and a steep growth of pressure beyond the full compaction point, the envelope of the pressure distributions shows three maximum values that are located at some distance away from the axis of symmetry opposed to a single peak at the axis of symmetry, as is the case for a distant explosion. This effect is more pronounced for the medium having sharper pressure growth in the EOS beyond the full compaction point and for smaller charge standoff distance.

The pressure distributions analysis reveals that the second (absolute-primary) and third (secondary) peaks are caused by the Mach stem effect appearing in a soil medium with full locking. The Mach stem is first developed at the point, that corresponds to the primary maximum and later it is developed at the point, corresponding to the secondary maximum. Therefore, it may be concluded that this secondary maximum of the peak pressure envelope corresponds to the secondary Mach stem phenomenon that does not appear in the case of a planar wall, where the incident angle depends on the wave front curvature only.

The development of the first peak requires further studies that are beyond the scope of this paper.

Acknowledgments

This work was supported by a joint grant from the Centre for Absorption in Science of the Ministry of Immigrant Absorption and the Committee for Planning and Budgeting of the Council for Higher Education under the framework of the KAMEA Program.

References

[1] Rakhmatulin KhA, Dem'yanov YuA. Strength under high transients loads. NY: Daniel Davey; 1966.
[2] Smith PDJG, Hetherington JG. Blast and ballistic loading of structures. Oxford: Butterworth Heinemann; 1994.
[3] Bulson PS. Explosive loading of engineering structures. London: Spon Press; 1997.
[4] Luccioni B, Ambrosini D, Nurick G, Snyman I. Craters produced by underground explosions. Comp Struct 2009;87:1366–73.
[5] Wlodarczyk E. Reflection of a stationary shock wave from a rigid partition in a three-component medium. J Tech Phys 1982;23:309–22.
[6] Wang ZHao, HLu Y. A three-phase soil model for simulating stress wave propagation due to blast loading. Int J Numer Anal Meth Geomech 2004;28:33–56.
[7] Lyakhov GM, Okhitin VN. Plane waves in nonlinear viscous multicomponent media. J Appl Mech Tech Phys 1977;18:241–8.
[8] Hurty WC, Rubinstein MF. Dynamics of structures. London: Prentice-Hall; 1964.
[9] Belytchko T, Hughes TJR. Computational methods for transient analysis. Amsterdam: North-Holland; 1983.
[10] Zienkiewich OC. The finite element method. London: McGraw-Hill; 1977.
[11] Lewis RW, Pettess P, Hinton E. Numerical methods in coupled systems. Chichester: Wiley&Sons; 1984.
[12] Stevens DJ, Krauthammer T. A finite difference/finite element approach to dynamic soil-structure interaction modelling. Comp Struct 1988;29(2):199–205.
[13] Grujicic M, Pandurandan B, Cheeseman BA. The effect of degree of saturation of sand on detonation phenomena associated with shallow-buried and ground-laid mines. Shock Vib 2006;13:1–21.
[14] Lyakhov GM, Osadchenko RA, Polyakova NI. Plane waves in nonhomogeneous media and their interaction with obstacles. J Appl Mech Tech Phys 1969;10:559–66.

[15] Baylor JT. Parameters affecting loads on buried structures subjected to localized blast effects. Army Eng. Waterways Exp.Station, Vicksburg MS Structures Lab; 1992.
[16] Luccioni B, Ambrosini D, Yuen SCK, Nurick G. Effects of large and spread explosives loads. Int J Prot Struct 2010;1:319–44.
[17] Feldgun VR, Kochetkov AV, Karinski YS, Yankelevsky DZ. Internal blast loading in a buried lined tunnel. Int J Impact Eng 2008;35:172–83.
[18] Yankelevsky DZ, Karinski YS, Feldgun VR. Re-examinations of shock wave's peak pressure attenuation in soils. Int J Impact Eng 2011;38:864–81.
[19] Wilkins ML. Fundamental methods in hydrodynamics. In: Alder B, Fernbach S, Rotenberg M, editors. Calculation of elastic-plastic flow. Methods in computational physics. NY: Acad. Press; 1964. p. 211–63.
[20] Miller GH, Colella P. A high-order Eulerian Godunov method for elastic-plastic flow in solids. J Comp Phys 2001;167:131–76.
[21] Washizu K. Variational methods in elasticity and plasticity. Oxford: Pergamon Press; 1968.
[22] Kim MK, Lim YM, Rhee JW. Dynamic analysis of layered half planes by coupled finite and boundary elelments. Eng Struct 2000;22:670–80.
[23] Karinski YS, Feldgun VR, Yankelevsky DZ. Explosion induced dynamic soil-structure interaction analysis with the coupled Godunov – variational difference approach. Int J Num Meth Eng 2009;77:829–54.
[24] Yankelevsky DZ, Feldgun VR, Karinski YS. Underground explosion of cylindrical charge near a buried wall. Int J Impact Eng 2008;35:905–19.
[25] Karinski YS, Feldgun VR, Racah E, Yankelevsky DZ. Mach stem due to an underground explosion near a rigid structure buried in soil. Shock Waves 2015;25(1):63–76.
[26] Karinski YS, Feldgun VR, Racah E, Yankelevsky DZ. The mach stem phenomenon for shaped obstacles buried in soils. In: Iványi P, Topping BHV, editors. Proceedings of the 9th International Conference on Engineering Computational Technology. Civil-Comp Press; 2014. p. 46. doi:10.4203/ccp.105.46.
[27] Ben-Dor G. Shock wave reflection phenomena. 2nd ed. Springer; 2007.
[28] Karinski YS, Feldgun VR, Yankelevsky DZ. Effect of soil locking on the cylindrical shock wave's peak pressure attenuation. ASCE J Eng Mech 2009;135:1166–79.
[29] Courant, R., Friedrichs, K.O., Supersonic flow and shock waves. NY: Interscience Publishers Inc.: 1967.
[30] Lee EL, Horning HC, Kury JW. Adiabatic expansion of high explosives detonation products TID 4500-UCRL 50422. Livermore: Lawrence Livermore National Laboratory of the University of California; 1968.